ESC European Society of Cardiology

Cardiovascular Research (2017) **113**, 1789–1797
doi:10.1093/cvr/cvx172

Low-energy defibrillation with nanosecond electric shocks

Frency Varghese[1,2†], Johanna U. Neuber[1,2], Fei Xie[3], Jonathan M. Philpott[4], Andrei G. Pakhomov[2], and Christian W. Zemlin[1,2*]

[1]Department of Electrical and Computer Engineering, Old Dominion University, Norfolk, VA, USA; [2]Center for Bioelectrics, Old Dominion University, 4211 Monarch Way, Norfolk, VA 23508, USA; [3]Department of Engineering, Mount Vernon Nazarene University, Mount Vernon, OH, USA; and [4]Department of Surgery, Eastern Virginia Medical School, Norfolk, VA, USA

Received 6 January 2017; revised 7 June 2017; editorial decision 12 August 2017; accepted 28 August 2017; online publish-ahead-of-print 29 August 2017

Time for primary review: 56 days

Aims Reliable defibrillation with reduced energy deposition has long been the focus of defibrillation research. We studied the efficacy of single shocks of 300 ns duration in defibrillating rabbit hearts as well as the tissue damage they may cause.

Methods and results New Zealand white rabbit hearts were Langendorff-perfused and two planar electrodes were placed on either side of the heart. Shocks of 300 ns duration and 0.3–3 kV amplitude were generated with a transmission line generator. Single nanosecond shocks consistently induced waves of electrical activation, with a stimulation threshold of 0.9 kV (over 3 cm) and consistent activation for shock amplitudes of 1.2 kV or higher (9/9 successful attempts). We induced fibrillation (35 episodes in 12 hearts) and found that single shock nanosecond-defibrillation could consistently be achieved, with a defibrillation threshold of 2.3–2.4 kV (over 3 cm), and consistent success at 3 kV (11/11 successful attempts). Shocks uniformly depolarized the tissue, and the threshold energy needed for nanosecond defibrillation was almost an order of magnitude lower than the energy needed for defibrillation with a monophasic 10 ms shock delivered with the same electrode configuration. For the parameters studied here, nanosecond defibrillation caused no baseline shift of the transmembrane potential (that could be indicative of electroporative damage), no changes in action potential duration, and only a brief change of diastolic interval, for one beat after the shock was delivered. Histological staining with tetrazolium chloride and propidium iodide showed that effective defibrillation was not associated with tissue death or with detectable electroporation anywhere in the heart (six hearts).

Conclusion Nanosecond-defibrillation is a promising technology that may allow clinical defibrillation with profoundly reduced energies.

Keywords Defibrillation • Stimulation • Nanosecond shocks • Millisecond shocks • Low-energy

1. Introduction

For decades, delivering intense electric shocks has been the principal life-saving intervention to terminate ventricular fibrillation. Adverse effects of defibrillation, especially at higher energy levels, may include increased morbidity and mortality, anxiety, pain, and cell damage.[1–3] The quest for more efficient yet safer defibrillation has brought the transition from monophasic to biphasic waveforms[4–6] and motivates the ongoing research into low-energy defibrillation strategies.[7,8]

Recent advances in pulsed power engineering and a better understanding of bioeffects of nanosecond shocks and nanosecond pulsed electric fields (nsPEFs) have pointed to nanosecond shocks as a potentially superior modality for defibrillation. Just like the conventional (millisecond-duration) electric shocks, nanosecond shocks can excite nerve and muscle cells.[9,10] However, nanosecond shocks do not rely exclusively on charge movement and redistribution to reach the threshold membrane voltage.[11] As a result, nanosecond shocks can more simultaneously excite the entire volume of cardiac tissue between the electrodes. Another result is a more uniform electric field distribution in myocardium, with greatly reduced impact of tissue inhomogeneities,[12] and reduced risk of induction of new wave fronts that can reinitiate VF.

Many adverse effects of defibrillation mentioned above are associated with electroporation.[3,13,14] Depending on the extent of electroporation (from mild to severe), cells depolarize and exhibit reduced action potential (AP) amplitude; lose intracellular K^+ and ATP; take up Na^+ and Ca^{2+}, with a multitude of downstream effects due to Ca^{2+} signalling;

* Corresponding author. Tel: +1 757 683 3745; fax: +1 757 451 1010, E-mail: czemlin@odu.edu

† Present address. University of Massachusetts Medical School, Worcester, MA, USA.

take up water, swell, and form membrane blebs; proceed to either apoptotic or necrotic death. At the same time, electroporation may be anti-arrhythmic and assist defibrillation.[3,13] Even when nanosecond shocks are electroporating, the effective diameter of membrane pores is limited to 1–1.5 nm[15,16–19] ('nanoelectroporation'), which minimizes the adverse effects from the loss and uptake of solutes while preserving the benefit of reduced excitability. This undesired transport of solutes is further reduced because the short shock duration essentially eliminates the electrophoretic component.[20]

Here, we demonstrate for the first time that nanosecond defibrillation is indeed possible. In Langendorff-perfused rabbit hearts, we were able to consistently both stimulate and defibrillate with nanosecond shocks. The associated defibrillation energy was about an order of magnitude lower than that of monophasic millisecond defibrillation.

2. Methods

2.1 Surgical preparation

The IACUC of Old Dominion University approved the animal protocols for the experiments reported here. All animal experiments were performed in accordance with the NIH guidelines (guide for the care and use of laboratory animals). New Zealand white rabbits of either sex (3–4 kg, $n = 18$) were heparinized (500 IU/kg) and brought to a surgical plane of anaesthesia with 3–4.5% isoflurane (inhalation). The heart was rapidly removed, the aorta cannulated and flushed with ice cold Tyrode solution (in mM: NaCl: 128.2, $NaCO_3$: 20, NaH_2PO_4: 1.2, $MgCl_2$: 1.1, KCl: 4.7, $CaCl_2$: 1.3, glucose: 11.1), and the heart was placed in a Langendorff-perfusion setup, where it was perfused and superfused with warm oxygenated Tyrode solution (37 ± 0.5 °C) at a constant pressure of 60–80 mmHg. After 30 min equilibration, 10–15 mM of 2,3-butanedione monoxime was added to eliminate contractions.

2.2 Optical mapping

Figure 1A shows a schematic of our optical mapping setup. A 1000 mW, 671 nm diode laser (Shanghai Dream Lasers) was directed through a 5° conical diffusor and then through a dichroic mirror (λ_{crit}=690 nm) onto the heart to achieve uniform illumination. Fluorescence light passed the dichroic mirror and a 715 nm long pass filter and was recorded with a CCD camera ('Little Joe', SciMeasure, Decatur, GA) at 1000 frames per second. *Figure 1B* shows the preparation in the setup, with plate electrodes touching the ventricular walls on both sides. An inset shows the special window electrode we fabricated for optical mapping of the area directly under the electrodes. This window electrode is an aluminium plate with a 5 mm hole in the centre; the hole is covered with a glass plate that is coated with indium tin oxide (ITO), so that the glass plate is both transparent and electrically conductive. Also, the ITO-covered glass plate is attached with electrically conductive glue, so that the window electrode presents a seamless conductive surface that is equivalent to the plate electrode without a window. By recording voltage-sensitive fluorescence through the electrode window, we are able to observe shock-induced electric activity right under the shock electrodes (where the effect of the shock should be strongest). This is particularly relevant when we look for signs of shock-induced damage. The window electrode was utilized in part of the stimulation/defibrillation experiments (see Results section, subsection 'Absence of baseline shift').

The preparation was stained with the near-infrared dye DI-4-ANBDQBS. A stock solution was made by dissolving 10 mg dye in 1.2 ml of pure ethanol; for each experiment, 30 µL of the stock solution was diluted with 15 mL of Tyrode's solution and injected as a bolus.

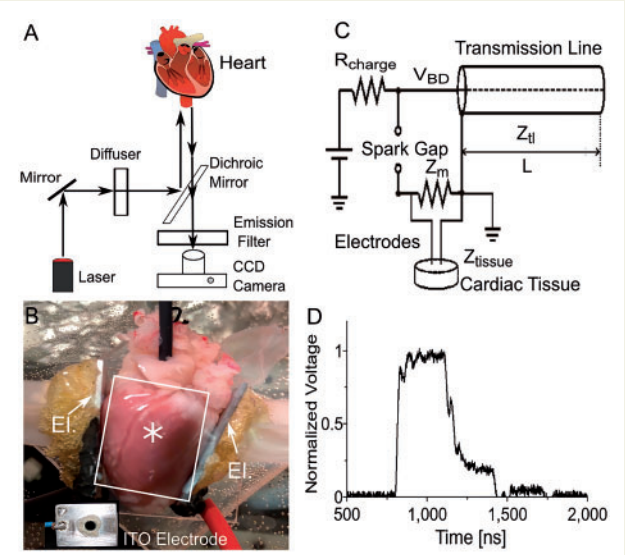

Figure 1 Setup used in our defibrillation experiments. (*A*) Optical mapping setup. The heart is stained with the voltage-sensitive fluorescent probe Di-4-ANBDQBS and illuminated with a diffused laser at 671 nm. Fluorescent light is filtered with a long pass filter and recorded with a CCD camera. (*B*) Photograph of heart in setup. The electrodes are positioned to the left and to the right of the heart (see arrows labelled 'El.'), illumination is from the top, and fluorescent light is also recorded from the top. Two aluminium plate electrodes touch the heart at the right and left ventricular free wall. Inset shows indium tin oxide (ITO) window electrode for observation of shock effects right under the electrode. A circular hole was drilled into the aluminium electrode and covered with glass that was coated with (electrically conductive) ITO. The label 'asterisks' indicates where the ITO electrode was located when it was used. The white rectangle indicates a typical field of view of the camera. (*C*) Spark gap generator for 300 ns shocks. (*D*) Experimentally determined shock waveform.

2.3 Induction of ventricular fibrillation

Ventricular fibrillation was induced in some hearts ($n = 12$) by touching the ventricular surfaces with two electrodes connected to the poles of a 9 V battery, and gently moving the electrodes on the cardiac surface. This generally induced fibrillation. Fibrillation was considered sustained when it lasted at least 30 s after the battery had been removed. In some hearts (8 out of 12), fibrillation consistently self-terminated after less than 30 s; in these hearts, 5–10 µM pinacidil was added to shorten the action potential and make sustained fibrillation more likely. In this way, we were able to induce sustained fibrillation in all hearts.

2.4 Nanosecond shock generation, stimulation, and defibrillation

Nanosecond shocks were created with a transmission line generator (see *Figure 1C*), which are well established in the field of 'Pulsed Power' (see Ref. [21,22] for a comprehensive discussion). Seven parallel, double-shielded coaxial cables (RG-217 U) were coiled and used as a transmission line capacitor ($C = 21.2$ nF measured). An additional resistor $Z_m = 13.7\ \Omega$ was placed in parallel with the heart to achieve impedance

matching between the transmission line and the load. In theory, this setup should charge the transmission line until the breakdown voltage of the spark gap is reached and apply rectangular shocks of duration $t=2l/v$ to the load, where l is the length of the transmission line and v is the speed of light in the transmission line. In our case, $l=30$ m, $v=0.66c$ (c is the speed of light in vacuum), and consequently, $t \approx 300$ ns (see *Figure 2B*). The actual shock shape was recorded with an oscilloscope (Tektronix 1001B, Beaverton, OR) and followed the theoretical prediction with good accuracy (see *Figure 1D*).

Stimulation shocks were applied to hearts in sinus rhythm. The shock was detected with an inductive loop placed close to the spark gap; the inductive loop was connected to an analogue/digital converter whose output was written into a corner pixel of our optical mapping movies as they were recorded. In this way, each movie contains the information in which frames shocks were applied.

Defibrillation shocks were applied to hearts that were exhibiting sustained ventricular fibrillation. All movies were checked for signs of spontaneous reversion to sinus rhythm.

2.5 Determination of stimulation/defibrillation threshold

When determining stimulation and defibrillation thresholds, we generally started at field strengths that were expected to be below the threshold and then progressively increased the field strength, up to the strengths that were consistently effective.

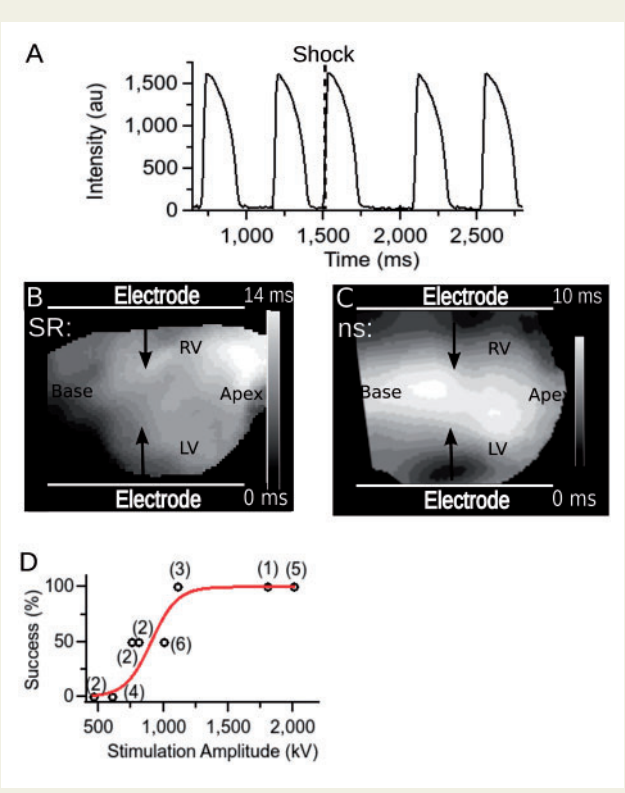

Figure 2 Stimulation of cardiac tissue with nanosecond shock (5 hearts). (*A*) Optical recording from a representative location on the cardiac surface. The heart is initially in sinus rhythm, before a single shock is applied at the time marked with a dashed line. Afterwards, sinus rhythm continues. (*B*) Activation map for sinus activation. (*C*) Activation map following nanosecond shock activation. (*D*) Stimulation success rate as a function of stimulus amplitude. Numbers in parentheses indicate how many observations contributed to each of the data points. Red line shows a sigmoidal function fitted to the data.

2.6 Computation of defibrillation energies

For millisecond shocks, we used a Pearson probe (Model 6585) to measure the current delivered to the fibrillation heart. We recorded both this defibrillation current and the field strength and integrated their product to obtain the deposited energy ($E=\int I(t)U(t)dt$). For nanosecond shocks, we used the fact that the shock energy is supplied by a capacitor that is completely discharged in the process ($E=\frac{CU_C^2}{2}$), where C is the capacitance of the capacitor and U_C is the charging voltage of the capacitor).

2.7 TTC/PI staining and sectioning

In a separate set of experiments ($n=6$ additional hearts, also New Zealand white rabbit), the effect of a single 3 kV, 300 ns shock on tissue viability, and the degree of electroporation were assessed with tetrazolium chloride (TTC) and propidium iodide (PI) stains.

Treated hearts were perfused with PI for 10 min. Five minutes into the PI perfusion, they received the shock so that they were perfused with PI before, during, and after shock application, to ensure that even transient permeability of the membrane for PI would be captured. In control hearts, we injected 50 µl Triton X-100 (5%) into the ventricular wall (Triton is a surfactant that effectively kills cells). Afterwards, we perfused with PI for 10 min (no shock was applied). In all cases, PI was washed out for 20 min.

All preparations were partially frozen to facilitate sectioning (30 min at -20 °C), sectioned into ~2 mm thick slices and immersed in TTC (30 mM/20 min), for further study of the geometry of the ablated volume. TTC stains metabolically active tissue deeply red, while dead cells appear white.[23]

3. Results

3.1 Stimulation with nanosecond shocks

Rabbit hearts could consistently be stimulated with a single nanosecond shock of 1.2 kV and higher (over 3 cm). *Figure 2*, Panel A, shows a representative trace from optical mapping of a heart in sinus rhythm to which one shock of 1.2 kV has been applied. Note that the action potential amplitude and shape are indistinguishable from those of sinus beats. Panel B shows the activation map for sinus activation. In contrast, Panel C shows the activation map following nanosecond stimulation, which is markedly different and reveals that the earliest activation occurs at the electrodes and that the whole tissue is activated within 10 ms. Panel D shows statistics on the stimulation threshold in a set of hearts ($n=5$). Stimulation was consistently effective for shocks of 1.2 kV or higher (over 3 cm). We fitted the stimulation success rate with a sigmoidal function and used it to estimate the stimulation threshold (defined as the field strength leading to 50% stimulation success) to be approximately 900 V (over 3 cm).

3.2 Defibrillation with nanosecond shocks

We were able to consistently defibrillate rabbit hearts with a single nanosecond shock of 3 kV (over 3 cm). *Figure 3A* shows a representative trace from optical mapping of a successful defibrillation. It is apparent that the fast irregular activity before the shock (fibrillation) is immediately interrupted by the shock and replaced by sinus rhythm. *Figure 3B* shows how the defibrillation success rate depends on the applied shock

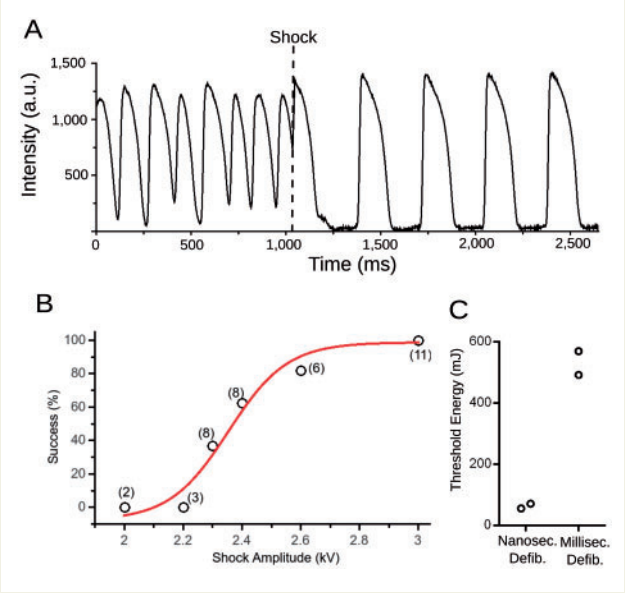

Figure 3 Defibrillation with nanosecond shock (12 hearts). (*A*) Optical recording from a representative surface location on the cardiac surface. The heart is initially fibrillating, before a single shock is applied at the time marked with a dashed line. After the shock, sinus rhythm is restored. (*B*) Defibrillation success rate as a function of stimulus amplitude. Numbers in parentheses indicate how many observations contributed to each of the data points. Red line shows a sigmoidal function fitted to the data. (*C*) Comparison of defibrillation for millisecond defibrillation (monophasic) and nanosecond defibrillation (2 hearts, see text for comparison with previous data regarding the energy threshold of millisecond defibrillation). Black empty circles indicate the threshold energies that we determined in individual hearts. Grey horizontal lines mark averages and standard error of the mean.

strength. The general shape of the dependence is familiar from conventional defibrillation, with no success up to 2.2 kV, increase success probability in the range 2.3–2.6 kV, and consistent success (11/11) for 3 kV. The fitted sigmoid curve corresponds to a defibrillation threshold (i.e. 50% defibrillation success) of 2.35 kV.

3.3 Comparison of required defibrillation energies: nanosecond versus millisecond defibrillation

The most commonly used measure for comparison of the efficacy of different defibrillation modalities is the energy required for defibrillation. Our defibrillation threshold of 2.35 kV allows the computation of the delivered threshold energy (see Methods section), which turns out to be 58.5 mJ. This is a remarkable reduction compared to the defibrillation energy required for millisecond defibrillation, which a previous study in Langendorff-perfused rabbit hearts, determined to be 270 mJ,[24] or approximately five times more than our threshold energy. The reduction by a factor of five occurred even though the cited study used smaller electrodes directly sutured to the free ventricular walls, which should be more effective for defibrillation, so that the true reduction should be by more than a factor of five.

To confirm in our setup that nanosecond defibrillation has a lower defibrillation energy threshold than conventional (millisecond) defibrillation, we determined the defibrillation threshold both for nanosecond defibrillation and conventional defibrillation in the same heart with the same electrode configuration ($n = 2$). Millisecond defibrillation was performed with monophasic-truncated exponentials of 10 ms duration. The defibrillation threshold was 2.3 kV ± 0.2 kV for nanosecond defibrillation and 37 ± 2 V for conventional defibrillation. As shown in *Figure 3C*, the associated energies were 530 ± 35 mJ for millisecond defibrillation and 64 ± 4 mJ for nanosecond defibrillation, i.e. nanosecond defibrillation required only 13% of the energy of millisecond defibrillation.

In units of stimulation thresholds, nanosecond defibrillation required ~2.6 stimulation thresholds for defibrillation (2.35 kV/0.9 kV), while millisecond defibrillation required 4.9 stimulation thresholds (37 V/7.5 V).

3.4 Mechanism of nanosecond defibrillation

To shed light on the mechanism of nanosecond defibrillation, we discuss a representative example. *Figure 4* shows a series of snapshots of the distribution of transmembrane voltages before, at, and after shock application. Panels A and B document the re-entrant activity prior to shock application. The shock application (Panel C) leads to an artefact, likely reflecting an effect of the shock on the camera. In this case, the artefact increases the signal at the centre of the image and persists for approximately 5 ms. In other examples, we observed artefacts that either increased or decreased the signal, either locally or globally, but in no case did the artefacts preclude the determination whether the heart returned to sinus rhythm after the shock. Panel D shows that 7 ms after the shock, the heart is uniformly depolarized. The whole field of view then goes through a synchronized action potential, which ends at 178 ms with complete repolarization (Panel E). The remaining Panels F–H show that the following activation is a typical sinus activation, with signal levels rising uniformly over a short time (10 ms).

3.5 Histological assessment of tissue damage due to nanosecond defibrillation

Four hearts were exposed to a single 300 ns-shock of 3 kV/cm, the shock strength that had 100% defibrillation success rate. Two control hearts were not exposed to any shocks but were locally injected with 5% Triton X-100 to demonstrate that the histological staining performed as expected. All 6 hearts were sectioned and analyzed for tissue death and electroporation using TTC and PI stains. *Figure 5* shows a sample treated heart, in which TTC staining was uniform and there was no PI staining; the same TTC/PI results were obtained in the remaining three treated hearts. This means that nanosecond shocks that are effective for defibrillation cause no detectable tissue death or electroporation sufficient for PI entry. Since the hearts were PI-perfused while the shock was applied, there was not even detectable transient electroporation.

In the control hearts, TTC staining was uniform except around the injection site of the Triton X-100. Likewise, there was no PI fluorescence anywhere besides the triton injection sites. This confirms that both TTC and PI stain performed as expected.

3.6 Absence of baseline shift

While histology shows that all tissue remains viable after nanosecond shock application, it is still a concern that the electrophysiology of the exposed tissue might be altered. The most obvious concern is significant electroporation that can be detected in optical mapping as a prolonged baseline shift (seconds to minutes) of the signal for affected pixels (because the cells are depolarized for the time during which the pores

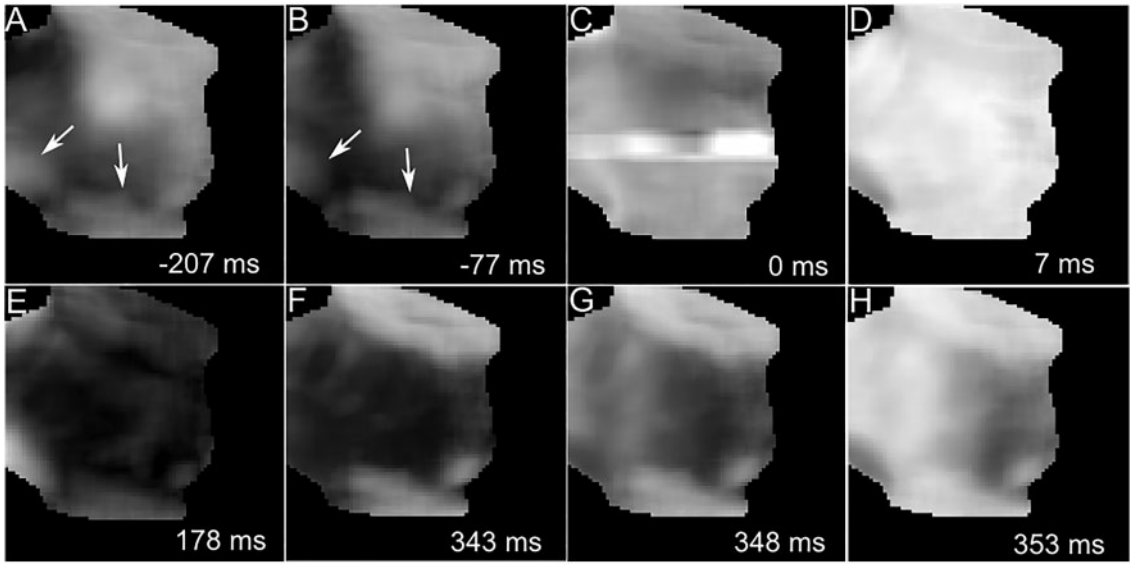

Figure 4 Mechanism of nanosecond defibrillation. Panels *A–H* show a series of snapshots of transmembrane voltage distribution, before (*A*, *B*), at (*C*), and after (*D–H*) the application of a nanosecond shock to a heart that exhibits re-entry. Dark areas are at resting transmembrane potential, bright areas are depolarized. White numbers in the lower right corner state the time the snapshot was taken, relative to the shock application (negative numbers mean that the snapshot was taken before the shock). White arrows indicate the direction of wave propagation.

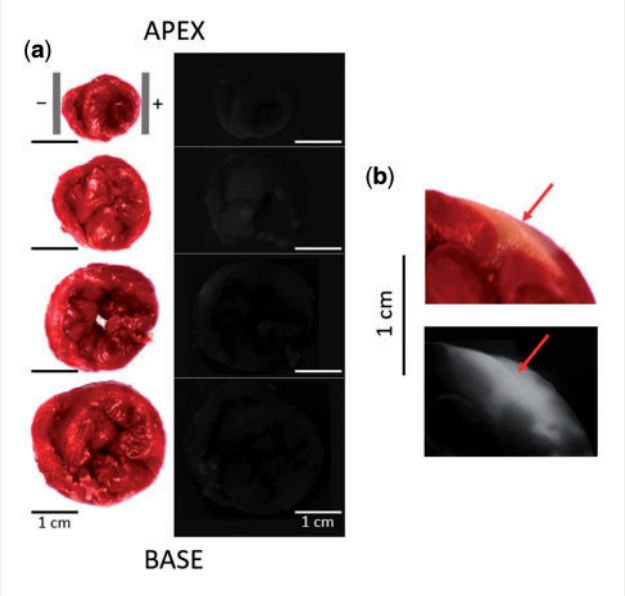

Figure 5 Histological assessment of tissue damage after a single 300 ns, 3 kV shock. (*A*) Side-by-side view of TTC stains (left) and PI fluorescence imaging (right) for a series of four coronal sections of the heart, arranged from apex (top) to base (bottom). The grey vertical bars in the top left panel indicate the electrode positions. The PI fluorescence is so weak that cardiac tissue is hardly discernable. All images are oriented with the left ventricle on the right side of the image. (*B*) Positive control using a 50 µl Triton X-100 injection. Injection site is marked with a red arrow in both the TTC stain (top) and the PI fluorescence image (bottom).

persist). We reviewed all our successful defibrillation recordings and checked for baseline shift but found no indication of it. To be able to assess baseline shift right below the shock electrodes, we developed special electrodes with an ITO window (*Figure 1B*) that allow us to record the shock response right under the shock electrode. With these electrodes, we recorded 35 shock responses (between 1 and 1.5 kV over 3 cm) in one heart. In our analysis of the responses, we did not see any sign of baseline shift.

3.7 Effect of nanosecond stimulation/defibrillation on action potential duration and diastolic interval

Another important test to see whether the shock affects the electrical activity of the heart is to see whether important characteristics of electrical activity, such as action potential duration (APD) or diastolic interval (DI) are different before and after the shock. This question also has a spatial component, as it may reasonably be assumed that tissue close to the electrodes is more affected by applied shocks that tissue that is further away.

In *Figure 6*, we show our results regarding the effects of nanosecond stimulation on APD and DI. As shown in Panel A, APD_{pre} denotes the duration of the action potential before the action potential immediately preceding the shock (the duration of the action potential directly preceding the shock is not a good comparison because this action potential may get interrupted by the shock). APD_{stim} is the duration of the shock-induced AP and APD_{post} the duration of the following AP. Similarly, we call the diastolic interval preceding the shock DI_{pre}, the first diastolic interval following the shock DI_{post}, and the next diastolic interval after that $DI_{post,\,2}$.

Panel B shows how we selected the points for evaluating APDs and DIs to address the question of spatial variation. The solid white lines mark the electrode positions, the black lines mark the position of the evaluation points (the evaluation points are in the centres of the black lines). The positions are identified by a number from 1 to 10 (shown in white).

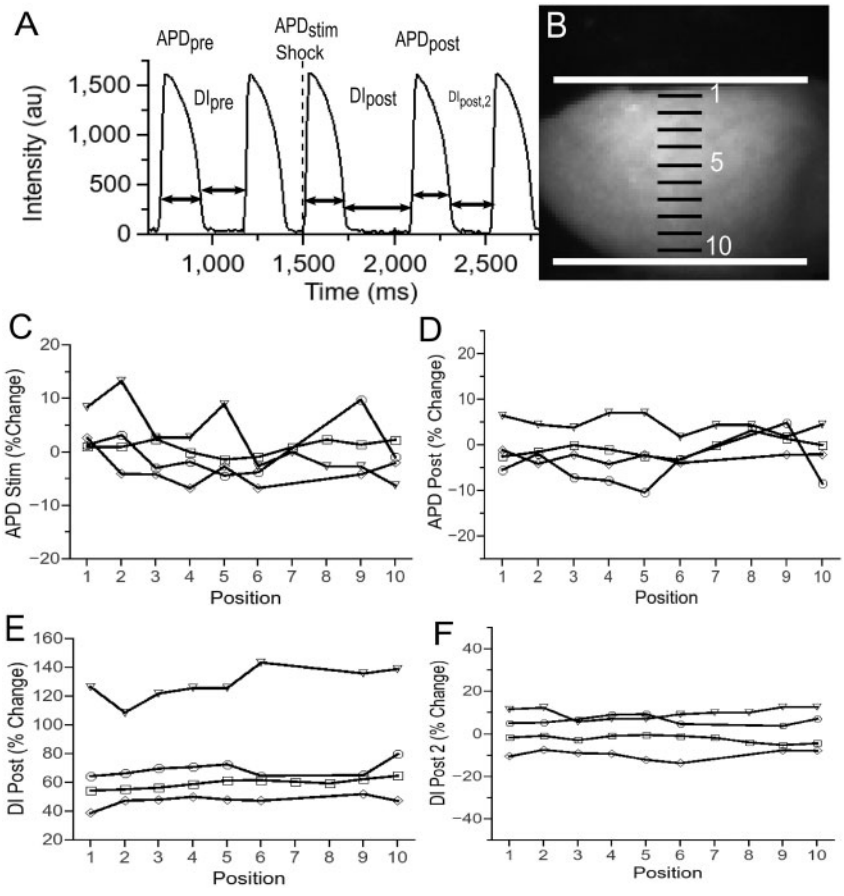

Figure 6 Effect of nanosecond stimulation on action potential duration and diastolic interval (4 hearts). (*A*) Sample optical recording from cardiac surface to introduce our notation (DI_pre, APD_pre, APD_stim, DI_post, APD_post, and DI_post, 2). (*B*) Photograph of heart in setup, with superimposed positions of shock electrodes and sample locations for the evaluation of APD and DI. (*C*) Change of APD_stim (relative to APD_pre) as a function of electrode position for 4 hearts. Different symbols ('inverted triangle', 'diam', 'open circle', and 'open square') represent different hearts. (*D*) Change of APD_post (relative to APD_pre) as a function of electrode position for 4 hearts. (*E*) Change of DI_post (relative to DI_pre) as a function of electrode position for 4 hearts. (*F*) Change of DI_post, 2 (relative to DI_pre) as a function of electrode position for 4 hearts.

Panel C evaluates how much APD_{stim} differs from APD_{pre} (10 positions per heart, 4 episodes in 4 hearts). We note that the vast majority of the observation points show a change of APD below 5%, with a handful of observation points in the range 5–10% and a single observation point above 10%. The average change was 0.2149% (SD 4.60%). These variations are on the same order as the variations from beat to beat in hearts that are not exposed to electric shocks: Performing the same analysis of APD variations in consecutive sinus beats (no shocks, 10 positions per heart, 8 episodes in 3 hearts), we find that the average change yielded an average change of -0.523% (SD 2.045%). Also note that there is no systematic bias of the changes towards certain electrode positions. In particular, there is no evidence for stronger effects close to the electrodes (Positions 1 and 10), which would be the most obvious concern.

Panel D compares APD_{post} to APD_{stim} (same episodes as Panel C), and the results are similar to those of Panel C. A large majority of the changes are below 5%, all others between 5% and 10% (average -0.57%, SD 4.45%), again consistent with variations in unshocked hearts, and no spatial pattern is observed.

Panel E compares DI_{post} with DI_{pre} (same episodes as Panel C). Here we do see a substantial change in all four hearts evaluated: The changes observed were between 40% and 140% (average 70.6%, SD 21.1%), all far above the typical variations for unshocked hearts (up to ≈ 10%). The spatial variations that change were small compared with the average change, and there we observed no spatial pattern.

Panel F compares $DI_{post,\ 2}$ with DI_{pre}. The differences are almost all below 10% (average 1.43%, SD 7.92), i.e. the increase observed in DI_{post} was temporary.

In *Figure 7*, we show our results regarding the effect of nanosecond defibrillation on DI (5 hearts). The terminology follows that of *Figure 6*, but introduces $DI_{post,\ 3}$ for the diastolic interval after $DI_{post,\ 2}$ (see Panel A). To evaluate the effect of the shock on the diastolic interval, we compared DI_{post} with $DI_{post,\ 2}$ (since no diastolic interval from before the shock was available). The results are shown in Panel B. We see that DI_{post} is substantially larger than $DI_{post,\ 2}$, with differences ranging from 30% to 100% (average 58.9%, SD 20.02%) and no discernable spatial pattern. For $DI_{post,\ 3}$, again compared with $DI_{post,\ 2}$, the differences are small (below 10%, average -1.514.%, SD 2.26%) and again do not show a spatial pattern. These results strongly suggest that the effect of the shock on the diastolic interval is transient, as in the case of nanosecond stimulation.

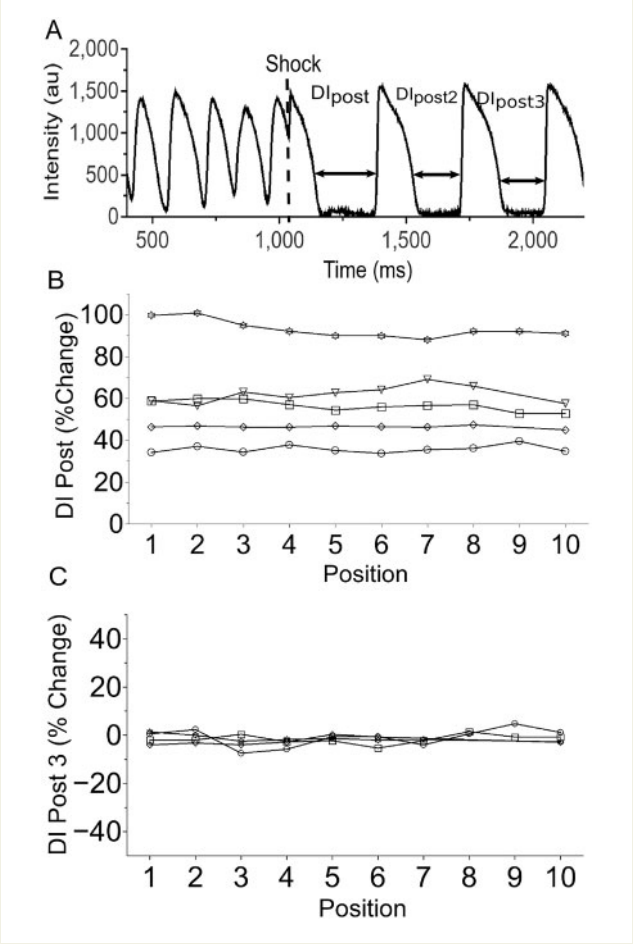

Figure 7 Effect of nanosecond defibrillation on diastolic interval (5 hearts). (*A*) Sample optical recording from cardiac surface to introduce our notation (DI_post, DI_post, 2, and DI_post, 3). (*B*) Change of DI_post (relative to DI_post, 2) as a function of electrode position for 5 hearts (same electrode positions as in *Figure 6*). Different symbols ('inverted triangle', 'diam', 'open circle', 'open star', and 'open square') represent different hearts. (*C*) Change of DI_post, 3 (relative to DI_post, 2) as a function of electrode position for 4 hearts.

4. Discussion

We have demonstrated the effectiveness of a new defibrillation modality, nanosecond defibrillation, which achieves reliable defibrillation with energies that are an order of magnitude smaller than those needed for conventional monophasic defibrillation. Additionally, in an isolated rabbit heart preparation, nanosecond defibrillation did not kill any tissue or electroporate it in a way that would cause detectable PI uptake. Nanosecond defibrillation did not cause a baseline shift in the optical transmembrane potential signal (which would indicate electroporation) or affect the action potential duration or shape. The diastolic interval following a shock-induced activation was notably prolonged, but only for a single beat.

All experiments were performed in isolated hearts with plate electrodes touching the ventricles; while this configuration generally requires far lower defibrillation energies than defibrillation with electrodes placed on the thorax, it is widely used because of the superior imaging possibilities that it offers and the fact that by adjusting the shock amplitude, fields comparable with clinical defibrillation (electrodes on the thorax) can be achieved.[25–28]

4.1 Mechanism of nanosecond defibrillation

External electric fields applied to the cardiac tissue induce local electric fields across the membrane of each cell in the tissue. In our approach, the external field is applied for nanoseconds rather than milliseconds, and it is not clear how such very short shocks induce a lasting change in the transmembrane potential.

Generally, the effects of an external field on the local transmembrane potential can be separated into two parts: the direct electric field, amplified by the heterogeneous permittivity (the amplification is quantified by a 'gain factor' g), and membrane charging due to the drift of ions the in the external electric field. The spread of the electric field and the gain due to heterogeneous permittivity (aligning of dipoles) occurs within the dielectric relaxation time $\tau=\epsilon_{cp}/\sigma_{cp}$,[29] where ϵ_{cp} is the permittivity of the cytoplasm and σ_{cp} is the conductivity of the cytoplasm. Typical values for the cytoplasm at body temperature, $\epsilon_{cp}=72.7\ \epsilon_0$ (ϵ_0 is the vacuum permittivity, $\epsilon_0 \approx 8.845 \cdot 10^{-12}$ F/m) and $\sigma_{cp}=1.7$S/m result in a relaxation time $\tau=378$ ps (similar for extracellular space, and blood/Tyrode solution), three orders of magnitude below our shock duration of 300 ns, so that we can conclude that the direct, amplified field is fully developed by the end of our shock.

Since the electric fields we use are only in the order 1 kV/cm, however, even a high estimate of the gain factor of 20 (see Ref. [30]) would lead to effective fields across the membrane of only ~20 kV/cm, or ~10 mV across a 5 nm membrane, sustained only for the duration of the shock. Such a transmembrane potential would be far too low to cause electroporation, and also too low to affect membrane channels, especially given the fact that it is only sustained for 300 ns.

The second mechanism by which our external fields induce transmembrane potential is membrane charging, the mechanism that is also responsible for millisecond defibrillation. It is well established that for 5–10 ms shocks, fields in the order of 1–2 V/cm are sufficient to excite cardiac tissue[31] and that fields in the order of 5 V/cm are sufficient to defibrillate.[32] Since the charging time constant for field in this amplitude range is in the low millisecond range,[33,34] such shocks achieve transmembrane charges close to the asymptotic level. Our external field is around 1 kV/cm, or around 200 times the defibrillation field of millisecond shocks, and it could be expected that a shock duration of 1/200 that of millisecond defibrillation, or around 25 μs, are required. It should be noted, however, that charging time drops substantially as the shock amplitude increased for millisecond shocks.[33,34] If the charging time constant does drop to values in the 10–100 μs range, membrane charging may account for the stimulation and defibrillation that we observe here.

The idea that nanosecond defibrillation works by charging the cell membrane is further supported by optical mapping data (see *Figure 4*) that show that nanosecond shocks uniformly activate the bulk of the tissue. We do not observe the strong virtual electrodes of both polarities that have been reported for millisecond shocks in experimental setups that closely resemble ours.[35]

Further experiments are needed to clarify the mechanism of nanosecond defibrillation. The charging time constant for large shock amplitudes is technically challenging to determine because of the fast imaging required, but previous work suggests that it is possible.[36]

4.2 Energy reduction compared to conventional defibrillation

Compared with monophasic conventional defibrillation, our nanosecond defibrillation approach achieved a reduction of defibrillation energy by almost an order of magnitude. This reduction is particularly impressive

when compared to the modest improvements yielded by the long transition from mono- to biphasic shocks (30–50% reduction[4–6]). The energy necessary for millisecond defibrillation determined by us (530 ± 35 mJ) is consistent with a previous studies in Langendorff-perfused rabbit hearts, which found 270 mJ for smaller electrodes directly sutured to the free ventricular walls,[24] an electrode configuration that would be expected to require less energy than ours.

It is an intriguing question why nanosecond defibrillation requires less energy than millisecond defibrillation. If the mechanism of nanosecond defibrillation is primarily membrane charging, as suggested above, and millisecond and nanosecond defibrillation would, therefore, share this mechanism, nanosecond shocks would need to be more effective at charging the membrane.

A possible explanation of greater charging effectiveness is that as the membrane is charged, leak currents, both through extracellular space and through the intracellular syncytium, become increasingly important; once the membrane is fully charged, all the current is lost as leak current. At the same time, shorter shocks require higher field strength, and since the energy lost in the leak current is, according to Ohm's law, proportional to the square of the field strength, there are competing effects of reducing shock duration on charging effectiveness. A better understanding of how the charging time constant changes with shock field strength is crucial to resolving these questions.

4.3 Tissue damage

We have evaluated a variety of markers for tissue damage, including shock-induced baseline shift, TTC staining for dead tissue, PI staining to detect electroporation, and spatially resolved parameters of cardiac electrical activity (APD and DI) before and after the shock. All of our results were consistent with the absence of any permanent tissue damage.

PI staining is the most commonly used technique to assess electroporative damage during defibrillation.[13,37,38] Two papers have assessed the electroporative damage caused by conventional (millisecond) defibrillation and have found that a shock of twice the threshold amplitude causes substantial PI uptake in the parts of the heart exposed to the strongest electric fields.

The only change in the electrophysiological behaviour that nanosecond stimulation and defibrillation caused was a prolonged first diastolic interval (50–100% longer) immediately after the shock. This result is in line with electric disturbances observed in cardiac tissue after millisecond shocks ('stunning')[39]; it is hardly a safety concern, especially since the diastolic interval goes back to normal by the second post-shock beat.

4.4 Limitations

This study is the first description of a new defibrillation modality and it is by necessity restricted to the most fundamental aspects of its efficacy and safety. An important question that we do not address here is the safety margin of nanosecond defibrillation shocks (how far above the defibrillation threshold do nanosecond shocks begin to cause damage). Also, while Langendorff-perfused hearts are a widely used model in defibrillation research, they do not allow the study of some important aspects of defibrillation, such as the effect of the thorax as a conducting volume around the heart in the case of defibrillation via body surface electrodes.

The current study is limited to single 300 ns shocks for defibrillation, and there is no reason to believe that it is the most effective pulsing scheme for nanosecond defibrillation. We chose single shocks because single shocks likely cause less complex phenomena than multiple shocks and lead to results that are easier to interpret and 300 ns shock duration because these are the shocks we have the most experience with. In order to assess the true potential of nanosecond defibrillation, the whole range of shock durations (1–1000 ns) should be explored and trains of shocks be considered as well. Previous research suggests that shorter nanosecond shocks can excite both muscle[9] and neurons,[40] and further substantial reductions in defibrillation energy may be possible.

Our assessment of tissue damage is limited to acute damage. It has been shown that nanosecond shocks can in certain settings induce apoptosis or other slower forms of cell damage.[11,41] It will be important to determine if such long-term tissue damage also occurs after nanosecond defibrillation and how it can be minimized.

Conflict of interest: A patent application for defibrillation with nanosecond shocks is pending, with A.G.P. and C.W.Z. as inventors.

Funding

This study was supported by supported by R01HL128381 from NHLBI (to A.G.P.).

References

1. Bradfield JS, Buch E, Shivkumar K. Interventions to decrease the morbidity and mortality associated with implantable cardioverter-defibrillator shocks. *Curr Opin Crit Care* 2012;**18**:432–437.
2. Cook SC, Marie Valente A, Maul TM, Amanda Dew M, Hickey J, Jennifer Burger P, Harmon A, Clair M, Webster G, Cecchin F, Khairy P. Shock-related anxiety and sexual function in adults with congenital heart disease and implantable cardioverter-defibrillators. *Heart Rhythm* 2013;**10**:805–810.
3. Al-Khadra A, Nikolski V, Efimov IR. The role of electroporation in defibrillation. *Circ Res* 2000;**87**:797–804.
4. Clark CB, Zhang Y, Davies LR, Karlsson G, Kerber RE. Transthoracic biphasic waveform defibrillation at very high and very low energies: a comparison with monophasic waveforms in an animal model of ventricular fibrillation. *Resuscitation* 2002;**54**:183–186.
5. Kudenchuk PJ, Cobb LA, Copass MK, Olsufka M, Maynard C, Nichol G. Transthoracic incremental monophasic versus biphasic defibrillation by emergency responders (TIMBER): a randomized comparison of monophasic with biphasic waveform ascending energy defibrillation for the resuscitation of out-of-hospital cardiac arrest due to ventricular fibrillation. *Circulation* 2006;**114**:2010–2018.
6. Mittal S, Ayati S, Stein KM, Knight BP, Morady F, Schwartzman D, Cavlovich D, Platia EV, Calkins H, Tchou PJ, Miller JM, Wharton JM, Sung RJ, Slotwiner DJ, Markowitz SM, Lerman BB. Comparison of a novel rectilinear biphasic waveform with a damped sine wave monophasic waveform for transthoracic ventricular defibrillation. ZOLL Investigators. *J Am Coll Cardiol* 1999;**34**:1595–1601.
7. Rantner LJ, Tice BM, Trayanova NA. Terminating ventricular tachyarrhythmias using far-field low-voltage stimuli: mechanisms and delivery protocols. *Heart Rhythm Off J Heart Rhythm Soc* 2013;**10**:1209–1217.
8. Luther S, Fenton FH, Kornreich BG, Squires A, Bittihn P, Hornung D, Zabel M, Flanders J, Gladuli A, Campoy L, Cherry EM, Luther G, Hasenfuss G, Krinsky VI, Pumir A, Gilmour RF, Bodenschatz E. Low-energy control of electrical turbulence in the heart. *Nature* 2011;**475**:235–239.
9. Rogers WR, Merritt JH, Comeaux JA, Kuhnel CT, Moreland DF, Teltschik DG, Lucas JH, Murphy MR. Strength–duration curve for an electrically excitable tissue extended down to near 1 nanosecond. *IEEE Trans Plasma Sci* 2004;**32**:1587–1599.
10. Wang S, Chen J, Chen M-T, Vernier PT, Gundersen MA, Valderrábano M. Cardiac myocyte excitation by ultrashort high-field pulses. *Biophys J* 2009;**96**:1640–1648.
11. Schoenbach KH, Hargrave SJ, Joshi RP, Kolb JF, Nuccitelli R, Osgood C, Pakhomov A, Stacey M, Swanson RJ, White JA, Xiao S, Zhang J, Beebe SJ, Blackmore PF, Buescher ES. Bioelectric effects of intense nanosecond pulses. *IEEE Trans Dielect Electr Insul* 2007;**14**:1088–1109.
12. Gowrishankar TR, Weaver JC. An approach to electrical modeling of single and multiple cells. *Proc Natl Acad Sci U S A* 2003;**100**:3203–3208.
13. Nikolski VP, Efimov IR. Electroporation of the heart. *Eur Eur Pacing Arrhythm Card Electrophysiol J Work Groups Card Pacing Arrhythm Card Cell Electrophysiol Eur Soc Cardiol* 2005;**7** (Suppl. 2): 146–154.
14. Tung L. Detrimental effects of electrical fields on cardiac muscle. *Proc IEEE* 1996;**84**:366–378.
15. Gowrishankar TR, Weaver JC. Electrical behavior and pore accumulation in a multicellular model for conventional and supra-electroporation. *Biochem Biophys Res Commun* 2006;**349**:643–653.

16. Bowman AM, Nesin OM, Pakhomova ON, Pakhomov AG. Analysis of plasma membrane integrity by fluorescent detection of Tl(+) uptake. *J Membr Biol* 2010;**236**:15–26.
17. Pakhomov AG, Bowman AM, Ibey BL, Andre FM, Pakhomova ON, Schoenbach KH. Lipid nanopores can form a stable, ion channel-like conduction pathway in cell membrane. *Biochem Biophys Res Commun* 2009;**385**:181–186.
18. Nesin OM, Pakhomova ON, Xiao S, Pakhomov AG. Manipulation of cell volume and membrane pore comparison following single cell permeabilization with 60- and 600-ns electric pulses. *Biochim Biophys Acta* 2011;**1808**:792–801.
19. Pakhomov A, Pakhmova O. A distinct transmembrane passageway in electroporated cells. In: AG Pakhomov, D Miklavcic, MS Markov (eds). *Advanced Electroporation Techniques in Biology and Medicine*. Boca Raton, FL: CRC Press; 2010.
20. Smith KC, Weaver JC. Transmembrane molecular transport during versus after extremely large, nanosecond electric pulses. *Biochem Biophys Res Commun* 2011;**412**:8–12.
21. Mesyats G. *Pulsed Power*. 1st ed. US: Springer; 2005.
22. Haddad M, Warne D (eds). *Advances in High Voltage Engineering*. London: The Institution of Engineering and Technology; 2009.
23. Bohl S, Medway DJ, Schulz-Menger J, Schneider JE, Neubauer S, Lygate CA. Refined approach for quantification of in vivo ischemia-reperfusion injury in the mouse heart. *Am J Physiol Heart Circ Physiol* 2009;**297**:H2054–H2058.
24. Holley LK, McCulloch RM. Comparison of biphasic and monophasic defibrillation waveforms in an isolated rabbit heart preparation. *Cardiovasc Res* 1991;**25**:979–983.
25. Hwang G-S, Tang L, Joung B, Morita N, Hayashi H, Karagueuzian HS, Weiss JN, Lin S-F, Chen P-S. Superiority of biphasic over monophasic defibrillation shocks is attributableto Less Intracellular Calcium Transient Heterogeneity. *J Am Coll Cardiol* 2008;**52**:828–835.
26. Ambrosi CM, Ripplinger CM, Efimov IR, Fedorov VV. Termination of sustained atrial flutter and fibrillation using low voltage multiple shock therapy. *Heart Rhythm* 2011;**8**:101–108.
27. Boukens BJ, Efimov IR. A century of optocardiography. *IEEE Rev Biomed Eng* 2014;**7**:115–125.
28. Efimov IR, Nikolski VP, Salama G. Optical imaging of the heart. *Circ Res* 2004;**95**:21–33.
29. Schoenbach KH, Xiao S, Joshi RP, Camp JT, Heeren T, Kolb JF, Beebe SJ. The effect of intense subnanosecond slectrical pulses on biological cells. *IEEE Trans Plasma Sci* 2008;**36**:414–422.
30. Semenov I, Xiao S, Kang D, Schoenbach KH, Pakhomov AG. Cell stimulation and calcium mobilization by picosecond electric pulses. *Bioelectrochemistry Amst Bioelectrochemistry* 2015;**105**:65–71.
31. Zemlin CW, Mironov S, Pertsov AM. Near-threshold field stimulation: intramural versus surface activation. *Cardiovasc Res* 2006;**69**:98–106.
32. Koster RW, Dorian P, Chapman FW, Schmitt PW, O'grady SG, Walker RG. A randomized trial comparing monophasic and biphasic waveform shocks for external cardioversion of atrial fibrillation. *Am Heart J* 2004;**147**:e20.
33. Mowrey KA, Cheng Y, Tchou PJ, Efimov R. Kinetics of defibrillation shock-induced response: design implications for the optimal defibrillation waveform. *Eur Eur Pacing Arrhythm Card Electrophysiol J Work Groups Card Pacing Arrhythm Card Cell Electrophysiol Eur Soc Cardiol* 2002;**4**:27–39.
34. Mowrey KA, Efimov IR, Cheng Y. Membrane time constant during internal defibrillation strength shocks in intact heart: effects of Na^{+} and Ca^{2+} channel blockers. *J Cardiovasc Electrophysiol* 2009;**20**:85–92.
35. Efimov IR, Aguel F, Cheng Y, Wollenzier B, Trayanova N. Virtual electrode polarization in the far field: implications for external defibrillation. *Am J Physiol Heart Circ Physiol* 2000;**279**:H1055–H1070.
36. Silve A, Rocke S, Frey W. Image processing for non-ratiometric measurement of membrane voltage using fluorescent reporters and pulsed laser illumination. *Bioelectrochem Amst Neth* 2015;**103**:39–43.
37. Kim SC, Vasanji A, Efimov IR, Cheng Y. Spatial distribution and extent of electroporation by strong internal shock in intact structurally normal and chronically infarcted rabbit hearts. *J Cardiovasc Electrophysiol* 2008;**19**:1080–1089.
38. Wang YT, Efimov IR, Cheng Y. Electroporation induced by internal defibrillation shock with and without recovery in intact rabbit hearts. *Am J Physiol Heart Circ Physiol* 2012;**303**:H439–H449.
39. Deakin CD, Ambler JJS. Post-shock myocardial stunning: a prospective randomised double-blind comparison of monophasic and biphasic waveforms. *Resuscitation* 2006;**68**:329–333.
40. Jiang N, Cooper BY. Frequency-dependent interaction of ultrashort E-fields with nociceptor membranes and proteins. *Bioelectromagnetics* 2011;**32**:148–163.
41. Pakhomova ON, Gregory BW, Semenov I, Pakhomov AG. Two modes of cell death caused by exposure to nanosecond pulsed electric field. *PLoS One* 2013;**8**:e70278.

Corrigendum

doi:10.1093/cvr/cvx184
Online publish-ahead-of-print 23 September 2017

Corrigendum to: Calmodulin/CaMKII inhibition improves intercellular communication and impulse propagation in the heart and is antiarrhythmic under conditions when fibrosis is absent [*Cardiovasc Res* 2016;**111**(4):410–421]

'We described in the Methods section that BDM was used at 100 mM. However, this was an error. In our experimental setting, BDM was always used at the concentration of 15 mM as previously described [1–4]. We sincerely apologize for this inconsistency and the inconvenience it may have caused.'

References

1. Yamazaki M, Honjo H, Nakagawa H, Ishiguro YS, Okuno Y, Amino M, Sakuma I, Kamiya K, Kodama I. Mechanisms of destabilization and early termination of spiral wave reentry in the ventricle by a class III antiarrhythmic agent, nifekalant. *Am J Physiol Heart Circ Physiol* 2007;**292**:H539–48.
2. Ishiguro YS, Honjo H, Opthof T, Okuno Y, Nakagawa H, Yamazaki M, Harada M, Takanari H, Suzuki T, Morishima M, Sakuma I, Kamiya K, Kodama I. Early termination of spiral wave reentry by combined blockade of Na+ and L-type Ca2+ currents in a perfused two-dimensional epicardial layer of rabbit ventricular myocardium. *Heart Rhythm* 2009;**6**:684–92.
3. Nakagawa H, Honjo H, Ishiguro YS, Yamazaki M, Okuno Y, Harada M, Takanari H, Sakuma I, Kamiya K, Kodama I. Acute amiodarone promotes drift and early termination of spiral wave re-entry. *Heart Vessels* 2010;**25**:338–47.
4. Takanari H, Honjo H, Takemoto Y, Suzuki T, Kato S, Harada M, Okuno Y, Ashihara T, Opthof T, Sakuma I, Kamiya K, Kodama I. Bepridil facilitates early termination of spiral-wave reentry in two-dimensional cardiac muscle through an increase of intercellular electrical coupling. *J Pharmacol Sci* 2011;**115**:15–26.